R. Steijl[1],F. Dehaeze[2],G.N. Barakos[3],
L.I. Garipova[4], A.N. Kusyumov[5], A.S. Mikhailov[6]
1 – 3 University of Liverpool,
4 – 5 KNRTU-KAI, Kazan,
E-mail: 1 - R.Steijl@liverpool.ac.uk, 2 - Florent.Dehaeze@liverpool.ac.uk,
3 - g.barakos@liverpool.ac.uk, 4 – lyaysan_garipova@mail.ru,
5- postbox7@mail.ru, 6 -sergey.mikhaylov@kai.ru

Simulation of flow around oscillating rotor blade section with aeroelastic flap

Keywords: rotor blade section, active flap, aeroelasticity, computational fluid mechanics (CFD)

Abstract

Flows around rotor blade sections equipped with active flaps are considered in this work. At certain flow conditions, and for certain flap structural properties, flutter or limit cycle oscillations of the flap may occur. In this paper, a method is demonstrated for the analysis of the flow around a flapped rotor blade section with a degree of freedom in the flap deflection angle. Results for oscillating flaps are presented. The resultant flap motion was found to couple with the unsteady air loads for cases of blade section in oscillatory translation.

1. Introduction

This paper presents an aeroelastic analysis of a rotor blade section equipped with a flap with one-degree-of-freedom (1-DOF).

For aerodynamic design of the rotors, vortex models [1, 2] are widely used. Modern and more complex approaches for modeling rotor performance are,

however, based on solutions of the Reynolds averaged Navier-Stokes equations with different turbulence models (see, for example, papers [3, 4] in Russian references).

The analysis of flapped rotors has so far been attempted by several authors and with a variety of modelling techniques. Amongst these works, authors of [5 - 8] employed a range of comprehensive methods that allow for some aspects of the flap to be modelled. Works with full Navier-Stokes based CFD also appear in the literature. The work [9] shows several techniques including local mesh refinement and adaptation near the flap. The use of over-set mesh techniques for a range of applications was demonstrated in [10], including an airfoil-flap-slat test case.

In addition to the numerical studies, the potential of reducing rotor vibrations by active flaps on blades recently was investigated in wind-tunnel tests [11]. For the closed-loop control system, a notable reduction in vibratory air-loads was reported. Without exception, all the above works identify potential issues related to the aeroelasticity of the flap and the effect of the flap structural properties in the overall rotor performance. The overall objective of the current work is to develop an appropriate method for modeling flap aeroelasticity within the framework of Navier-Stokes CFD methods and establish the best coupling strategy for the aerodynamics and structural analysis. In earlier efforts to couple CFD and structural analysis, the integration of the governing equations in time has been studied (see [12]) and several works exist presenting results for wing sections with one, two and some times more degrees of structural freedom. An example of these works can be found in [13, 14]. For blade sections of rotors in forward flight, the tangential velocity and blade pitch change periodically as the blade rotates. In the present work, these effects are modeled for two-dimensional sections using a periodic pitch oscillation and longitudinal translation. Other authors [15] only considered the Mach number variation, while most of the works focused on variations of the pitch angle of blade sections [13] In addition, the present work has a flap modelled using a servo-elastic method.

The work presented in this paper, employees the Helicopter Multi-Block solver of the University of Liverpool. A previous paper [16] presented the flap

model, and CFD results for flows around the steady rotors blade section equipped with aero-elastic flaps. The validation of the HMB code, the basic mathematical models and numerical schemes of the 1-DOF problem, its non-dimensionalisation, and the implementation of the algorithm were also detailed in [16]. The present paper can be considered as further work building on the method reported in [16] and shows CFD results for an oscillating blade section equipped with the aero-elastic flap.

2. Test cases description for 1-degree-of-freedom flap model -oscillating aerofoil

Table 1 presents the conditions of test cases for an oscillating OA209 airfoil. The airfoil oscillation schedule represents a blade section at 90%R span-wise position on the ONERA 7AD 4-bladed model rotor assuming a rotor tip Mach number Mtip = 0.60.The chord of the flap is 10% of the aerofoil chord. Test cases 1 and 2 assume constant pitch angle of 2.0^o and 4.0^o, respectively. The unsteady nature of the aerodynamics is purely the result of the translation (back and forth) of the section. Longitudinal coordinate x in this case is determined, by the expression $x = -\frac{v_\infty}{2k}\sin(2kt)$, were V_∞ is the free stream velocity, $2k$ is the rotor angular frequency. For all considered cases the rotor advance ratio was set to μ=0.333. The parameter μ_b (normalized blade mass for unit of the blade span) was also varied. Figure 1 shows the surface pressure distribution for test case 2, where the airfoil is assumed fully rigid, i.e. without flap deflection.

The formation of the strong normal shock for a part of the cycle corresponding to the advancing rotor side is apparent. The reduced dynamic head encountered by the section on the retreating side of the cycle leads to much lower air-loads through that part of the cycle.

Test cases, 3, 4a and 4b assume a representative pitch schedule defined by $\theta(2kt) = \theta_0 - \theta_{1S}\sin(2kt) - \theta_{1C}\cos(2kt)$, with $\theta_{1S} = 8.0^0$ and $\theta_{1C} = -2.0^0$. The parameter 2k determines the angular frequency of the rotor blade cyclic. For case 3,

θ_0=2.0°, while for 4a and 4b, θ_0 = 6.0°. Besides, the flaps for the test cases 4a and 4b are characterized by different eigen frequencies ω_0 [16].

Test case 3 has a negative pitch angle through parts of the advancing side, leading to the formation of a strong shock wave on the lower surface of the section. For a blade station at 90% R, this situation can arise in high-speed forward flight [17]. For test cases 4a and 4b, simulations were conducted in the different aero-elastic coupling methods and a wide range of different numerical parameters, as shown in Table 2.

3. Consistency and stability of different schemes

For the fixed-pitch test case 1, the predictions for the flap deflection angle from the leap-frog and direct implicit coupling methods [16] are compared in Figure2. The number of pseudo-steps for both cases was varied from 100 till 200. It can be seen that the results from the direct implicit coupling method converge well even for a small number of time-steps, i.e. for 720 or more (1440) time steps per translation cycle, the results are very close. The leap-frog method can also deliver good results that converge to the implicit solution at the expense of time steps. In general this results show that the direct implicit coupling method maybe more suitable for computations.

The results presented in Figure 2 indicate that for the leap-frog method, temporal convergence requires more time steps (2880) per translation cycle. For these cases, the results of the leap-frog methods for very smalltime-steps appear to approach those of the direct implicit coupling method.

This means that, both methods could be used effectively, however, with four times more steps per translation cycle required for the leap-frog method than for the direct implicit coupling method.

Test case 3, 4a and 4b were simulated using the direct implicit coupling method. Figures 3 and 4 show the predicted flap deflection angles. These figures

show also the solution obtained with the harmonic method [16], based on the development of solution in Fourier series.

The harmonic method only produced a stable solution when a single Fourier harmonic was used. For two or more Fourier modes in the harmonic method, resonance instability occurred. Also, the results for the direct implicit coupling method appear to be consistent with those for the 1-mode harmonic method at 1/cycle.

The results presented in Figures 3 and 4 indicate that for this challenging test case, well-resolved solution can be obtained with the direct implicit coupling method with 1440 steps per translation cycle. This temporal resolution is similar to what is used with HMB for computing rotors in forward flight.

4. Flap excitation during dynamic stall

For the rigid airfoil in cases 4a and 4b the stall would occur at identical conditions. The 1-degreeof-freedom flap aero-elastic model can be seen to give a significant flap deflection for the selected conditions. One of the effects of the flap deflection is a change of the efficient airfoil camber. During the part of the cycle associated with the ’retreating' side of a helicopter rotor disk, the highest angle of attack usually occurs around an azimuth of $2kt=270^{o}$. For the direct implicit coupling method, the flap schedule is shown in Figure 4. A large component at the harmonic nearest to the natural frequency of the flap can be observed for both natural frequencies of the flap. The main effect of the natural frequencies of the flap can be seen in the frequency content at higher frequencies as well as the phasing. The phasing of the flapping schedule will now largely determine whether, during the part of the cycle with the highest angle of attack, the camber of the airfoil can be reduced or increased. For the test cases 4a and 4b, the only difference is the flap eigen frequency ω_0 which for case 4a is 0.05, while it is 0.1 for case 4b. As can be seen from Figure 4(a) and 4(b), the flapping schedules for the two cases have similar amplitudes. Of course, the frequency content is significantly different.

On the ’retreating’ side, the phasing of the flapping excitation can be seen to be particularly different. In effect, the schedule obtained for case 4a has an upward flap deflection when the section enters the part of the cycle where stall is likely to occur. For case 4b, the opposite is true. Figure 5 shows the streamlines for the section as it passed through the retreating side of the cycle. The results are shown for a rigid section without flapping deflection. The formation of a strong dynamic stall vortex can be clearly seen. The sectional normal force as well as the sectional normal force for cases 4a and 4b is compared in Figure 6. For case 4a, the streamlines are shown in Figure 7, while case 4b is shown in Figure 8. As can be seen, the reduced airfoil camber in case 4a delays the stall onset relative to test case 4b. Comparing with the ’rigid’ section results, it can be seen that for both flapped cases, the onset of dynamic stall is delayed. The case with $\omega_0 = 0.05$ can be seen to also significantly reduce the extent of the stalled flow, while for the case with $\omega_0 = 0.1$ the addition of the flap motion did not reduce the extent of separated flow.

5. Conclusions

Computational analysis of the aero-elastic deflection of active trailing edges on rotor blade sections has been performed using a 1-degree-of-freedom flap model in the HMB CFD method. The aerodynamic environment of blade sections on a rotor in forward flight was approximated using a combination of an oscillatory translation and pitching motion, mimicking the effect of the tangential velocity changes and blade pitch schedule of blade sections on a rotor in forward flight, respectively.

The unsteady aerodynamics of the blades creates a time-dependent flap deflection. Various time integration methods for the 1-degree-of-freedom of the flap angle were investigated. The fully implicit coupling method was found to be the most reliable in predicting the flapping schedule. Time marching methods with a less direct coupling, i.e. the leap-frog method were found to give similar results to the fully implicit method when a much smaller time-step was used.

As an alternative to the time-marching methods, a harmonic balance method was also coupled to the time-marching CFD method. This method can be quite effective in establishing a time-periodic solution assuming an appropriate choice of an under-relaxation factor was used. However, the coupled harmonic balance time-marching CFD method was proved to be prone to develop resonance-type instability. To obtain a stable simulation, the number of Fourier modes needed to be cut-off the harmonic closest to the natural frequency of the flap. For stability analysis and accurate aerodynamics load evaluation, the method with direct implicit coupling appears to be the most reliable and accurate of the methods investigated in this work.

Acknowledgements

The financial support via the REACT project of AgustaWestland and the Business Innovation and Skills Department of the UK is gratefully acknowledged.

AK, LG and SM were supported via the “State tasks in the field of scientific activity” (No 9.1694.2014/K) grant.

References

1. *Anikin V. A., Gerasimov O. V., Kolomenski D. S., Kritski B. S., Sviridenko Yu. N.* Method of main rotor aerodynamics performances determination // Transaction of RosVO forum. 2004.

2. *Golovkin M.A., Golovkin V.A., Kalyavkin V.M.* Questions of vortex hydrodynamics / Under redaction of *Golovkin M.A.*, M. Physmatlit. 2009. – 264 p.

3. *Kosheev A.V.* Main rotor aerodynamics performances determination for hover and forward flights mode. —// TsAGI transactions. 2007, vol. 2673, Pp. 92 — 104.

4. *Ignatkin Yu. M., Konstantinov S.G.* Main rotor aerodynamics performances investigation using CFD method // Electronic journal «MAI transactions». Vol. № 57, 2012. – Pp. 1 – 22.

5. *Milgram J., Chopra I., Straub F.* Rotors with trailing edge flaps: Analysis and comparison with experimental data // Journal of the American Helicopter Society, pages 319–332, October 1988.

6. *Friedman P.P., Shanthakumaran P.* Optimum Design of Rotor Blades for Vibration Reduction in Rotorcraft in Forward Flight // 39th AHS Annual Forum, St. Louis, Missouri, USA, 1983.

7. *Shen J.* Comprehensive aeroelastic analysis of helicopter rotor with trailing edge flap for primary control and vibration control. PhD Thesis, University of Maryland, 2003.

8. *Cesnik C.E.S., Shin S-J., Wilbur M.L.* Dynamic response of active twist rotor blades // Smart Materials and Structures, 10:62–76, 2001.

9. *Jose A., Mishra A., Baeder J.* An investigation into the aerodynamics of tailing edge flaps with overhand and gap // AHS International Specialists' Conference on Aeromechanics, San Francisco, CA, USA, January 23-25, 2008.

10. *Sitaraman J., Floros M., Wissink A., Potsdam M.* Parallel domain connectivity algorithm for unsteady flow computations using overlapping and adaptive grids // Journal of Computational Physics, 229:4703–4723, 2010.

11. *Crozier P., Leconte P., Delrieux Y., Gimonet B., Le Pape A., H. Mercier des Rochettes*. Wind-Tunnel Tests of a Helicopter Rotor with Active Flaps // *32nd European Rotorcraft Forum*, Maastricht, the Netherlands, September, 2006.

12. *Friedman P.P., Gillot D., and Presente E.* Adaptive control of aeroelastic instabilities in transonic flow and its scaling // AIAA paper 97-0581, 1997.

13. *Barakos G.N., Drikakis D.* Numerical modelling of fluid-structure interaction problems // Chapter II-13 in Haase, W., Selmin, V. and Winzell, B. ed(s). Progress in Computational Flow-Structure Interaction, Berlin, Springer-Verlag, 2003.

14. *Dowell E.H.* A Modern Course in Aeroelasticity / 1st edition, Kluwer, 1995. 669 Pp.

15. *Владимирова Н. А.* Расчет аэродинамических характеристик винта вертолета на режиме висения и профилей в нестационарном потоке // Ученые записки ЦАГИ. Том XLVI. №1. 2015. Стр. 18-29.

16. *Стейл Р., Диизи Ф., Баракос Г., Гарипова Л.И., Кусюмов А.Н., Михайлов С.А.* Моделирование обтекания отсека лопасти с аэроупругим закрылком с одной степенью свободы // Изв. вузов. Авиационная техника. 2015. № 2. Стр. 54-59.

17. *Steijl R., Barakos G.N.* A Computational Study of the Advancing Side Lift Phase Problem // Journal of Aircraft, 45(1): 246–257, 2008.

Table 1: Test cases considered for 1 degree-of-freedom model

case	M_{mean}	μ	μ_b	ω_0	ζ	θ_0	θ_{1S}	θ_{1C}
1	0.5553	0.333	10	0.10	0.0	2.0°	0.0°	0.0°
2	0.5553	0.333	100	0.10	0.0	4.0°	0.0°	0.0°
3	0.5553	0.333	100	0.10	0.0	2.0°	8.0°	-2.0°
4a	0.5553	0.333	100	0.05	0.0	6.0°	8.0°	-2.0°
4b	0.5553	0.333	100	0.10	0.0	6.0°	8.0°	-2.0°

Table 2: Simulations performed

test case	method	steps/cycle	pseudo-steps	harmonics
2	Leap-frog	1440, 2880, 5760	50	-
	Direct-implicit	360, 720, 1440, 2880	50, 100	-
	Periodic	360	50	1
3	Leap-frog	360, 720, 1440, 2880	50	-
	Direct-implicit	360, 720, 1440	25, 50, 100	-
	Periodic	360, 720, 1440	50	1, 10
4a	Leap-frog	360, 720, 1440	50	-
	Direct-implicit	360, 720, 1440	25, 50, 100	-
	Periodic	360	50	1, 10
4b	Leap-frog	360, 720, 1440, 2880, 5760	50	-
	Direct-implicit	360, 720, 1440	25, 50, 100	-
	Periodic	360	50	1, 10

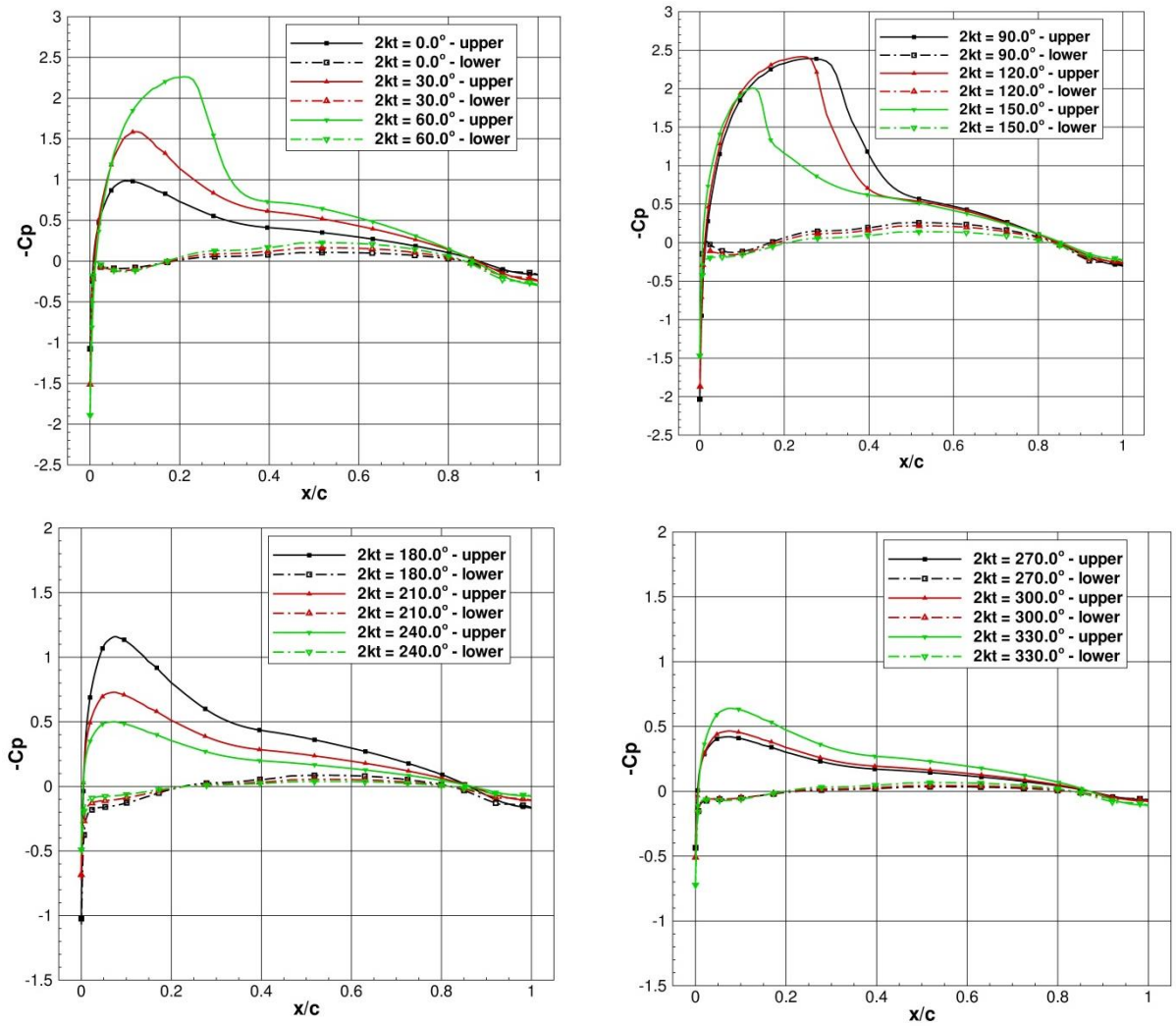

Figure 1: Surface pressure distribution. ONERA OA209 section in oscillatory translation. A rigid section is assumed with $\delta = 0^{o}$. Test case 2.

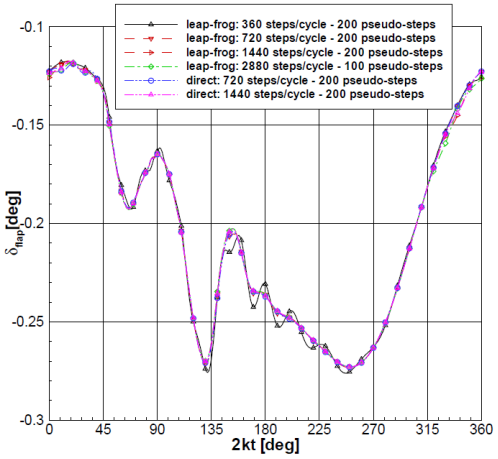

Figure 2: comparison of leap-frog and direct implicit coupling. Flap 1DOF aero-elastic model. ONERA OA209 section in oscillatory translation. Case 1

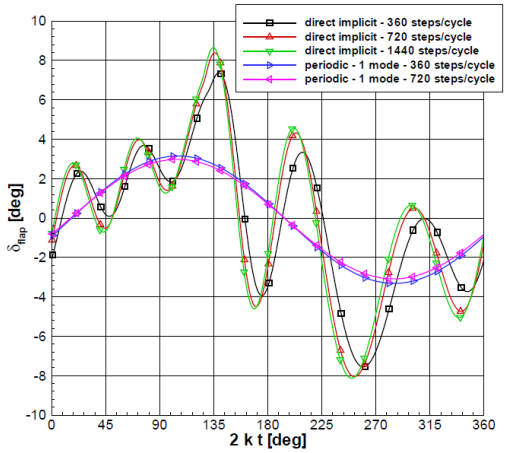

Figure 3: 1DOF aero-elastic flap model. Pitch schedule $\theta = 2.0^0 - 8.0^0 \sin(2kt) + 2.0^0 \cos(2kt)$ – Case 3

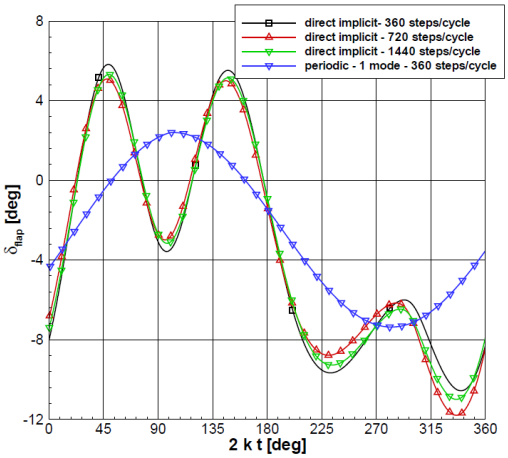

(a) $\omega_0 = 0.050$

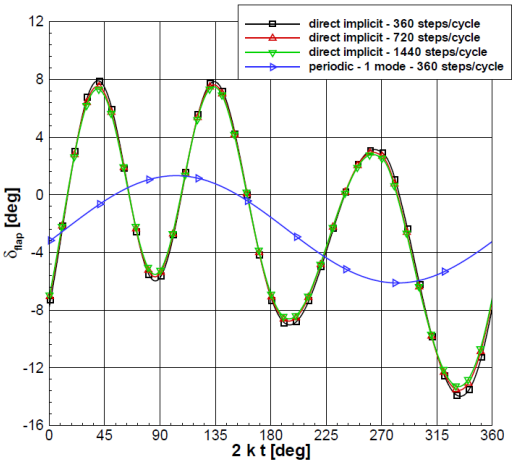

(b) $\omega_0 = 0.100$

Figure 4: 1DOF aero-elastic flap model. ONERA OA209 section in oscillatory translation. Pitch schedule $\theta = 6.0^0 - 8.0^0 \sin(2kt) + 2.0^0 \cos(2kt)$ - Cases 4 a, b

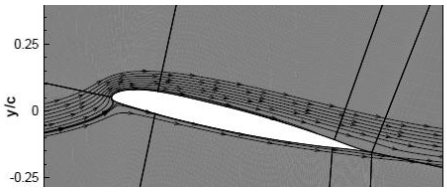

(a) 2*kt*= 240º

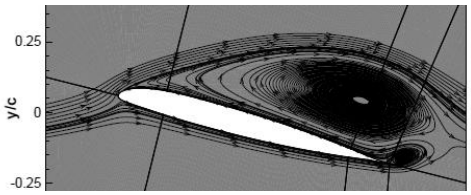

(b) 2*kt*= 270º

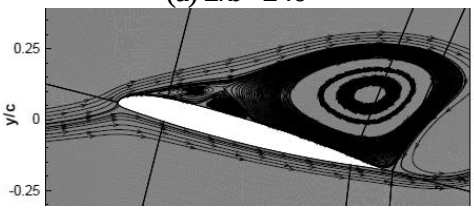

(c) 2*kt*= 280º

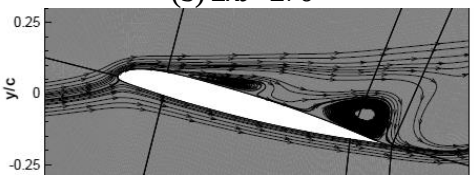

(d) 2*kt*= 290º

Figure 5: Streamlines. Rigid ONERA OA209 section without flapping deflection in oscillatory translation. Pitch schedule $\theta = 6.0^0 - 8.0^0 \sin(2kt) + 2.0^0 \cos(2kt)$

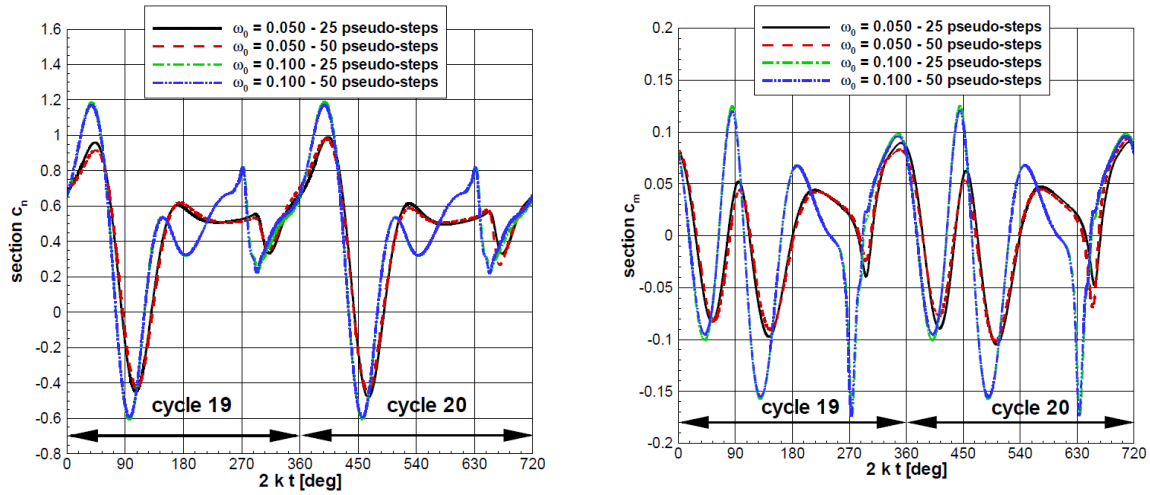

(a) sectional normal force (b) sectional pitching moment

Figure 6: 1DOF aero-elastic flap model. ONERA OA209 section in oscillatory translation. Pitch schedule $\theta = 6.0^0 - 8.0^0 \sin(2kt) + 2.0^0 \cos(2kt)$

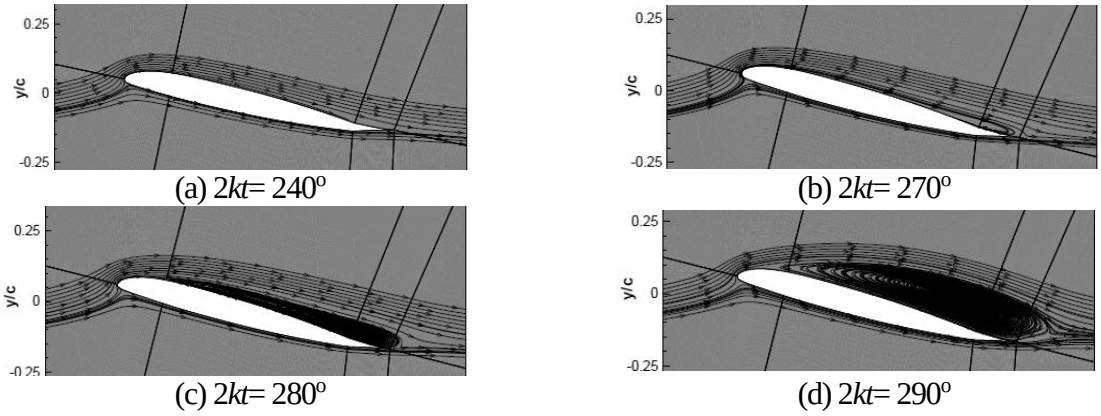

(a) 2*kt*= 240º (b) 2*kt*= 270º

(c) 2*kt*= 280º (d) 2*kt*= 290º

Figure 7: Streamlines. Flap 1DOF aero-elastic model. ONERA OA209 section in oscillatory translation. Pitch schedule $\theta = 6.0^0 - 8.0^0 \sin(2kt) + 2.0^0 \cos(2kt)$. $\omega_0 = 0.050$

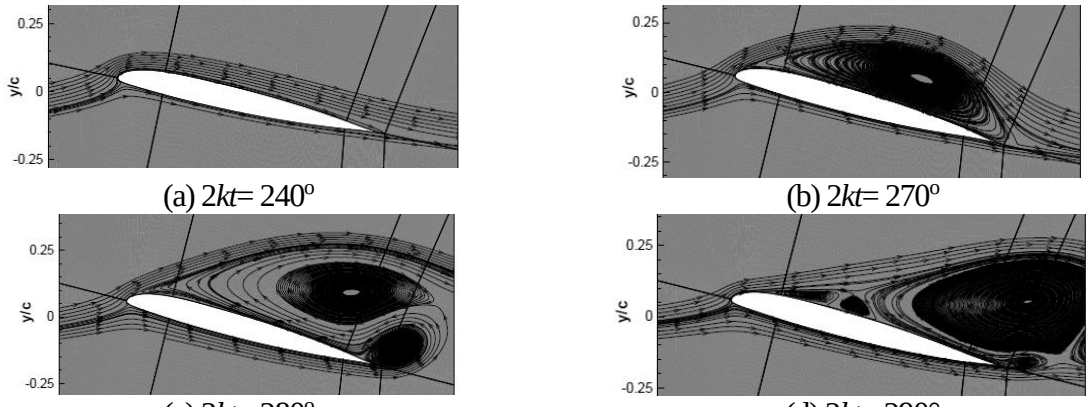

(a) 2*kt*= 240º (b) 2*kt*= 270º

(c) 2*kt*= 280º (d) 2*kt*= 290°

Figure 8: Streamlines. Flap 1DOF aero-elastic model. ONERA OA209section in oscillatory translation. Pitch schedule $\theta = 6.0^0 - 8.0^0 \sin(2kt) + 2.0^0 \cos(2kt)$. $\omega_0 = 0.100$